Dry biases in land water storage and excessive soil moisture limitation in CMIP6 models

Francesco Giardina[1], Ryan S. Padrón[1,2], Benjamin D. Stocker[3,4], Dominik L. Schumacher[1], Sonia I. Seneviratne[1]

[1]Institute for Atmospheric and Climate Science, Department of Environmental Systems Science, ETH Zurich, CH-8092 Zürich, Switzerland
[2]Swiss Federal Institute for Forest, Snow and Landscape Research WSL, CH-8903 Birmensdorf, Switzerland
[3]Institute of Geography, University of Bern, Hallerstrasse 12, 3012 Bern, Switzerland
[4]Oeschger Centre for Climate Change Research, University of Bern, Falkenplatz 16, 3012 Bern, Switzerland

Author for correspondence:
Francesco Giardina
Email: fgiardina@ethz.ch

Abstract

Accurate representation of plant water availability is crucial for climate modeling, due to its significant role in land-atmosphere interactions. Our study focuses on water storage dynamics and analyzes how soil moisture limitation is represented in Earth System Model (ESM) simulations of the Coupled Model Intercomparison Project phase 6 (CMIP6). We first quantify the long-term maximum annual depletion in water storage, contrasting model results with estimates based on satellite observations of terrestrial water storage from the Gravity Recovery and Climate Experiment (GRACE), as well as remotely sensed estimates of the water balance. Our analysis shows that CMIP6 models mostly underestimate the maximum annual soil moisture depletion, especially in the Amazon region. We further assess the frequency of soil moisture limitation in CMIP6 simulations against observations from solar-induced fluorescence (SIF) and GRACE, finding that ESMs generally overestimate this frequency. We obtain consistent results when comparing models to ground observations at 128 sites from the FLUXNET2015 dataset. Our study highlights the importance of improving the representation of plant water availability and land-atmosphere interactions in Earth System Models. Implementation of new model features could have large implications in predicting future climate on land.

Introduction

Climate projections are based on a variety of Earth System Model (ESM) simulations compiled in model intercomparison projects[1]. The accuracy of these simulations is key for progress in climate science and eventually affects the implementation of climate policies globally. The sixth phase of the Coupled Model Intercomparison Project (CMIP6) substantially contributed to the physical science basis of the Sixth Assessment Report (AR6) by the Intergovernmental Panel on Climate Change (IPCC)[1,2]. This phase includes the most advanced Earth System Models (ESMs), simulating historical and future climates based on greenhouse gas and aerosol concentration scenarios outlined in the Shared Socioeconomic Pathways (SSP)[3]. Nonetheless, continuous efforts are needed to keep improving multi-model ensembles, as some models have been shown to not fully align with observational evidence or theoretical understanding[4–6].

Soil moisture, a main component of the terrestrial water storage, links the global energy, water and carbon cycles, and is hence key for accurate climate projections[7–9]. By influencing the distribution of available energy at the land surface (conceptualized as net radiation), soil

moisture primarily directs this energy towards the evaporation of water[7,10]. This process not only affects the water cycle but also modulates the turbulent heat fluxes, thereby impacting the overall climate system[11]. Soil moisture acts as a reservoir for precipitation and radiation anomalies, maintaining stability in the climate system[10,12]. It regulates plant functions like transpiration and photosynthesis, impacting global water and carbon cycles[7]. When soil moisture drops below a critical threshold, evapotranspiration (ET) decreases, leading to an increase in sensible heating and ultimately in air temperature[10,11]. Water limitation is estimated to affect ET in 30% to 60% of the Earth's land surface for most of the year[13].
Despite the significant role of soil moisture and land-atmosphere interactions in controlling heat extremes, our understanding of the interactions among these components and their modulation by climate change is still limited[10]. This is reflected in the representation of land-atmosphere interactions in climate models[14,15]. Recent research has suggested an overestimation of future warming across CMIP6 models[5], plausibly connected to other documented biases in soil moisture[6] through land-atmosphere interactions. This uncertainty affects our ability to project our success in limiting global warming below the 2°C target outlined in the Paris Agreement. It is therefore crucial to constrain these model ensembles with other evidence, such as historical trends and current climate observations.
Using simulations from the land surface model component of seven ESMs within CMIP6[16], we show that total soil moisture storage is largely underestimated compared to observations, in particular in the Amazon. Consistently, we find that the frequency of water-limited conditions for evapotranspiration tends to be overestimated across models. We discuss the reasons behind these biases and the potential implications for climate projections and policy.

Biases in land water storage

We focus on the *Land-Hist* experiment within the Land Model Intercomparison Project (LMIP), which shares the same land model configuration of *historical* simulations within CMIP6[16]. LMIP consists of simulations from the land component of ESMs participating in CMIP6, driven by the same atmospheric forcing[16]. It provides observation-based historical reconstructions of snow and soil moisture at the global scale, thus allowing for more accurate assessments of water availability over continents across CMIP6 models[16]. These simulations are specifically designed to identify systematic biases in the representations of land processes in current ESMs[16].
We use total soil moisture data from seven ESMs within CMIP6[2] and terrestrial water storage

(TWS) observations from the Gravity Recovery and Climate Experiment (GRACE)[17]. Changes in TWS are used as a proxy for changes in total soil-water availability, as in previous studies[8,9,18]. The total soil moisture variable from LMIP includes moisture from all soil layers in the model (see Methods). Note that wherever in the manuscript we refer to "soil moisture" for brevity, we denote "total column soil moisture" as quantified by the variable defined within CMIP6 models.

In every grid cell, we estimate the maximum depletion of total-column soil moisture based on the greatest annual difference between the highest and lowest total-column soil moisture monthly values across all analyzed years:

$$\Delta SM_{max} = max(max(SM)_{year} - min(SM)_{year})_{all\ years} \quad (1)$$

This allows for the quantification of the maximum amplitude in total column soil moisture across all years of record (ΔSM_{max}). Our analysis thus focuses on land water storage that is active in land-atmosphere exchanges. We repeated the calculation for GRACE (ΔTWS_{max}). Our results show that the maximum soil moisture depletion is generally underestimated in CMIP6 models compared to observations, especially in the tropics (Fig. 1a,b). We obtain similar results when estimating total water storage with the maximum cumulative water deficit (CWD_{max}, Fig. 1c,d). The CWD is computed as the 80-year extreme of the seasonal maximum cumulative difference between evapotranspiration (ET) and precipitation (P). Assessment with CWD thus reveals patterns of water stress effects resulting from whole-column water depletion (see Methods). For the CWD calculation with CMIP6 data, we directly used ET and P from CMIP6 models. For the observational reference (henceforth referred to as S_{CWDX}), we used the 80-year extreme CWD from Ref.[19], determined using ET data derived from thermal infrared remote sensing via the Atmosphere Land Exchange Inverse (ALEXI) product[20,21] and precipitation reanalysis data from WATCH-WFDEI[22] (see Methods).

There is a potential for overestimating water storage when using GRACE data, particularly in regions prone to regular flooding, such as the Amazon, because the product accounts for all water bodies on land (i.e. rivers, lakes, water in vegetation, etc). However, using the CWD_{max} method and with ALEXI and WATCH-WFDEI datasets still indicates an overestimation of water storage in the Amazon (Figs. 1c, d and 2). On the other hand, S_{CWDX} tend to underestimate water storage when derived from ET obtained from infrared thermal remote sensing, which is often inaccurately low at high latitudes and regions that are not typically water limited (Fig. 1c). Ultimately, while no model or observational dataset provides a flawless comparison, the insights based on GRACE and ALEXI are valuable and generally point towards consistent findings (Figs. 1 and 2).

The mean bias in CMIP6 model outputs of CWD is lower when compared to S_{CWDX}, primarily due to a significant underestimation of water storage at higher latitudes when using this product (Fig. 1c). This underestimation leads to an increase in mean bias while substantially lowering the raw bias (i.e. the bias calculated simply as the mean of the differences between the model outputs and the corresponding observed values). In contrast, estimations derived from GRACE exhibit a lower susceptibility to such biases, increasing their reliability overall.

Generally, the consistency in patterns of exceptionally higher water storage within the wet tropics, as identified through both GRACE and S_{CWDX} observations (Fig. 1a,c), highlights the robustness of our finding that models underestimate water storage when compared with empirical data (Fig. 1b,d).

When grouping our results by IPCC regions, a clear model underestimation of water storage is apparent, especially in the tropics (Fig. 2). Using the S_{CWDX} and the $\mathrm{CWD}_{\mathrm{max}}$ method reveals further significant regions within the wet tropics where water storage is underestimated, extending beyond the Amazon to encompass areas in Africa, Australia, South Asia, and Central America (Fig. 2b).

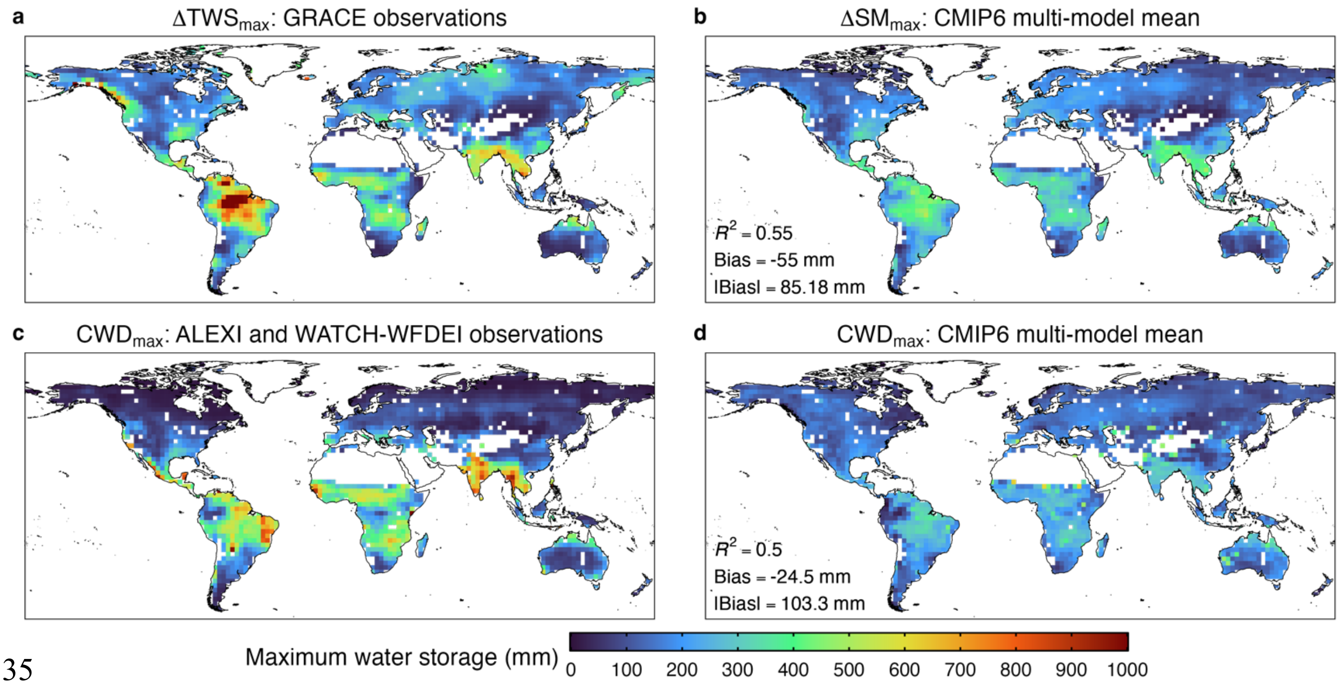

Fig. 1 | Comparison of total water storage estimates from CMIP6-LMIP simulations against observations-based estimates a-b, The maximum soil moisture depletion (ΔSM_{max}) was first derived yearly during 2003-2014. For every grid cell, we retained the maximum yearly reduction across those years. (**a**) ΔTWS_{max} from GRACE and (**b**) ΔSM_{max} from CMIP6. **c-d,** Total water storage estimated with maximum CWD (**c**), determined from ALEXI and WATCH-WFDEI observations (S_{CWDX}) augmented using an extreme value distribution with an 80-year return period, as detailed in Ref[19] and (**d**) maximum CWD assessed over the 80 years of CMIP6 data (1935-2014), to align with the methodology used for S_{CWDX}. The *land-hist* simulation was used across CMIP6 models. Bilinear interpolation was applied to harmonize the GRACE resolution with that of CMIP6. The raw bias was determined by subtracting pixel-by-pixel the observed value from each model and then calculating the mean of these differences across all pixels. For the absolute bias, we computed the mean after taking the absolute value of each pixel-wise subtraction. Values exceeding 1000 mm are colored as 1000 mm for clarity. The multi-model mean was calculated with models CESM2, CMCC-ESM2, CNRM-ESM2-1, E3SM-1-1, EC-Earth3-Veg, IPSL-CM6A-LR and UKESM1-0-LL.

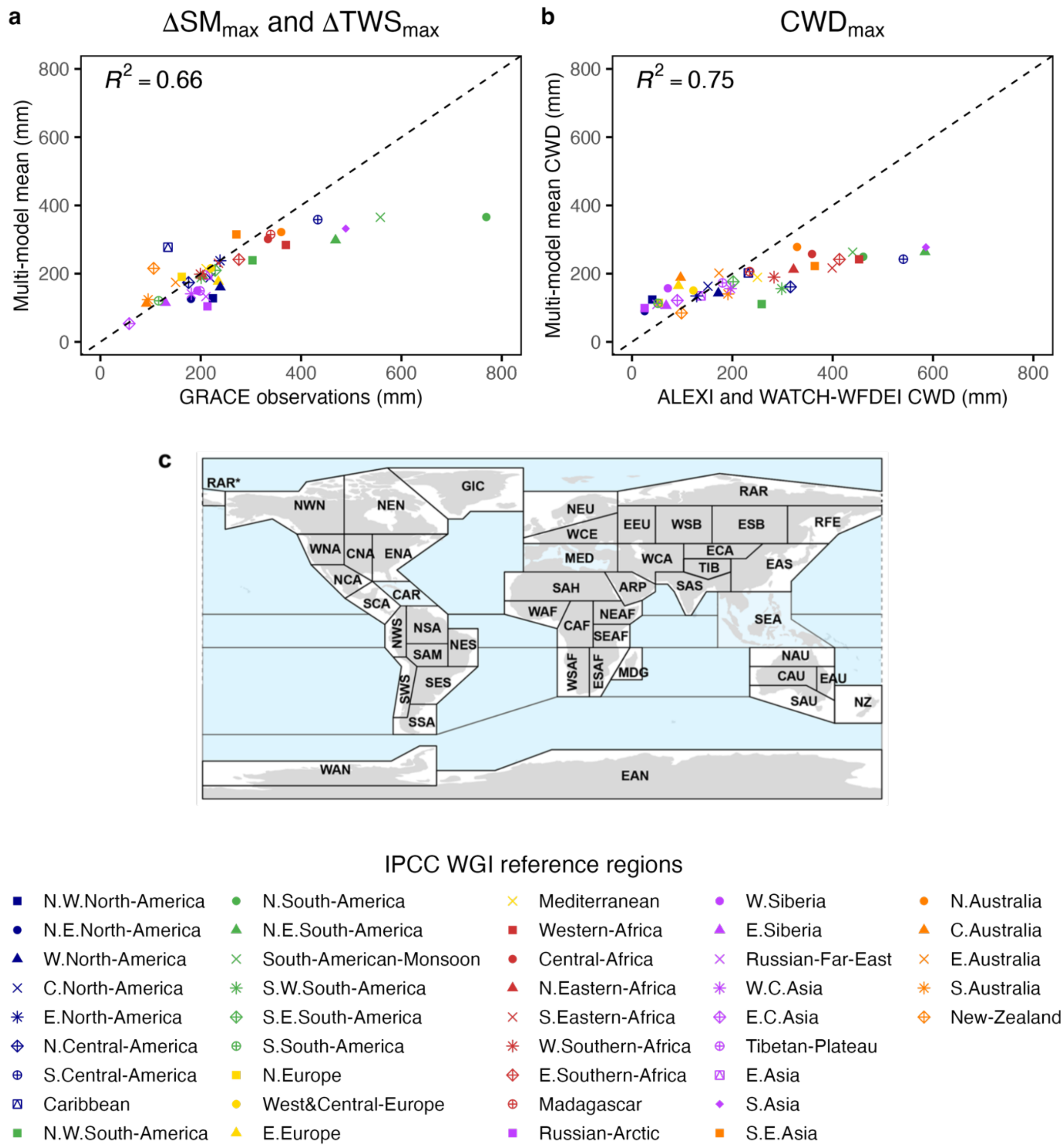

Fig. 2 | Comparative analysis of maximum soil moisture depletion across different IPCC regions based on LMIP-CMIP6 model simulations and observations. We present a region-wise evaluation of maximum soil moisture depletion, using observations-based estimates and corresponding LMIP-CMIP6 model simulations. **a**, ΔTWS_{max} from GRACE and ΔSM_{max} from CMIP6. **b**, Total water storage estimated with maximum CWD. **c,** IPCC reference regions. We first determined the maximum soil moisture depletion in every pixel and then we calculated the mean of this value within each IPCC region for model and observational data. The multi-model mean was calculated with models CESM2, CMCC-ESM2, CNRM-ESM2-1, E3SM-1-1, EC-Earth3-Veg, IPSL-CM6A-LR and UKESM1-0-LL.

Biases in soil moisture limitation

To quantify water constraints on photosynthesis, we study the evaporative fraction of net radiation (EF) as a function of the total-column soil moisture (see Methods). Given the complexities of measuring EF on a global scale, we use remotely sensed solar-induced fluorescence (SIF) observations as a proxy for EF, and terrestrial water storage (TWS) observations from GRACE as a proxy for total water storage. To calculate the frequency of soil moisture limitation, we first derive the soil moisture limitation threshold at every grid cell and subsequently compute the proportion of time each grid cell remains beneath this threshold (see Methods).

We find that the frequency of soil moisture limitation is generally overestimated in CMIP6 models compared to observations, especially in the wet tropics. Conversely, models often underrepresent the occurrence of water limitation in central and northern Europe and generally at high latitudes in the Northern Hemisphere (Fig. 3 and Supplementary Fig. 5). The finding that models significantly overestimate water limitation in the Amazon when compared to GRACE and GOME-2 data is further confirmed when performing the same analysis with FLUXNET2015 observations (Fig. 4 and Supplementary Fig. 8). This is a more direct comparison, as when focusing on FLUXNET2015 data we can work at daily timescales and directly calculate EF. We find that most ESMs assume that a humid biome as the Amazon has the same water limitation pattern as a dry Mediterranean savanna (Fig. 4).

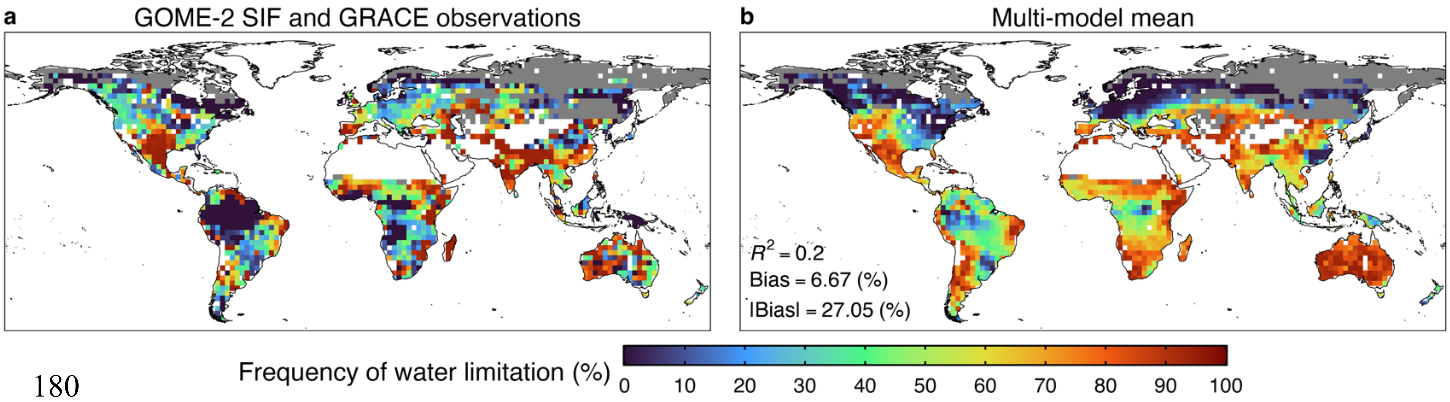

Fig. 3 | Global maps of frequency of soil moisture limitation. Pixel-specific critical soil moisture thresholds were first calculated to determine when plant water stress occurs. We then show the fraction of months with soil moisture below the critical threshold. **a,** Soil moisture thresholds determined with the normalized SIF versus normalized TWS from GRACE (2007-2014). **b,** Soil moisture thresholds calculated with EF vs normalized total column soil moisture with CMIP6 LMIP data (2007-2014). Dark blue pixels represent areas where no threshold could be determined by our algorithm, i.e. soil moisture is rarely limiting. On the other hand, dark red pixels represent areas that are almost always water limited. The raw bias was determined by subtracting pixel-by-pixel the observed value from each model and then calculating the mean of these differences across all pixels. Grey areas illustrate regions where the segmented regression could not be applied due to the scarcity of data points. For the absolute bias, we computed the mean after taking the absolute value of each pixel-wise subtraction. Details of all datasets and normalizations can be found in the Methods. The multi-model mean was calculated with models CESM2, CMCC-ESM2, CNRM-ESM2-1, E3SM-1-1, EC-Earth3-Veg, IPSL-CM6A-LR and UKESM1-0-LL.

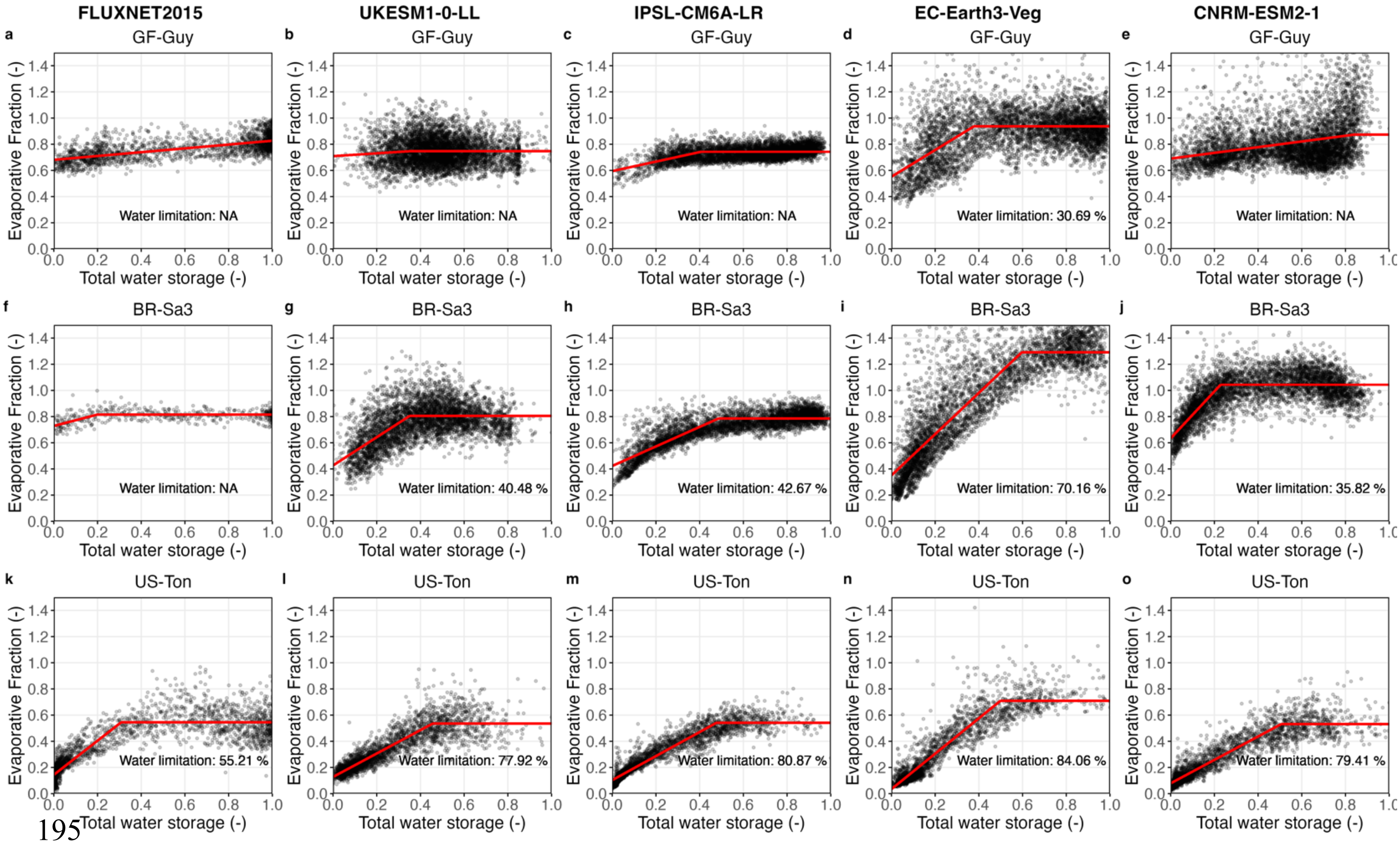

Fig. 4 | Analysis of soil moisture limitation at three selected eddy-covariance sites. a,f,k, eddy-covariance measurements from the FLUXNET2015 dataset. **b,g,l,** data from UKESM1-0-LL. **c,h,m,** data from IPSL-CM6A-LR. **d,l,n.** data from EC-Earth3-Veg. **e,j,o.** data from CNRM-ESM2-1. When the decrease in the EF was under 30% (as indicated by the y-axis intercept) compared to its maximum value, we assigned a status of no water limitation (NA). The total water storage was normalized to ease the comparison between model outputs and the corresponding observed values (see Methods). GF-Guy is an evergreen broadleaf forest site situated in the coastal region of the north-western Amazon, in French Guyana. BR-Sa3, another site characterized by evergreen broadleaf forest, lies further south and inland in Brazil. US-Ton is an oak savanna woodland located near Sacramento, California, United States.

Potential causes of biases between CMIP6 models and observations

Using both the ΔSM_{max} and CWD_{max} methods, we find that the total moisture storage is underestimated in models versus observations (Figs. 1 and 2). This suggests that models generally overestimate the occurrence of soil moisture limitation, as confirmed in Figs. 3 and 4 (i.e. the raw bias is positive for all models except CESM2). Given that soil moisture and ET are closely linked through land-atmosphere interactions[7,10], the underestimation of total soil moisture storage and overestimation of water limitation is consistent with previous studies suggesting that models overestimate the magnitude of ET reduction during droughts[23–26]. Europe and North America emerge among the least biased regions when compared to observations (Figs. 1-4). This is probably due to the large availability of ground-based observations to constrain ESMs in these areas compared to the rest of the world. At the same time, soil moisture storage appears to be most biased in the Amazon and in general in the wet tropics (Fig. 2). This is consistent with previous studies highlighting that ESMs overestimate water stress in the Amazon and fail to capture the positive sensitivity to atmospheric aridity in its most humid regions[27]. This also reflects the inadequate representation of tropical forest root traits found in global models[28]. Given the key role of the Amazon for the global water and carbon cycles[29,30], it is crucial that models accurately account for this region, also because the response of tropical rainforests to water stress is one of the main uncertainties in ESMs[31].

Among the seven CMIP6 models considered in this study, CESM2 has the most accurate representation of the soil-plant-atmosphere continuum[24,32,33]. It explicitly accounts for plant hydraulics and calculates water potentials in soil, roots, stems, and leaves[32]. This enables plants in CESM2 to draw more water for transpiration from deeper soil layers compared to other ESMs[32]. This explains why CESM2 is one of least biased models in the Amazon (Supplementary Fig. 3; see also table below) and overall the model with the lowest raw bias (Supplementary Figs. 1, 2, 5). CNRM-ESM2-1 and UKESM1-0-LL consistently rank as the models with lowest mean bias and highest linear fit for the spatial pattern (R^2, Supplementary Figs. 1, 2, 5). This is perhaps linked to the fact that they both simulate LAI dynamics instead of assuming a constant LAI seasonality and they account for vegetation properties and land use change (Supplementary Table 1). CNRM-ESM2-1 is one of the best existing ESMs in simulating deep soil moisture[6] and also accounts for feedbacks in the processes of the terrestrial carbon-cycle. EC-Earth3-Veg, while being one of the best models at estimating water storage (Supplementary Figs. 1 and 2), ranks as one of the least accurate in terms of water limitation (Supplementary Fig. 5). This discrepancy likely stems from its limited accuracy in simulating EF (Fig. 4).

Implications for predicting future climate on land

Our global comparison of seven state-of-the-art ESMs to observational estimates has revealed a tendency of underestimated total water storage and overestimated water limitation. In other words, these models generally *(i)* simulate less water potentially available for evaporation, and *(ii)* limit evaporation more frequently in response to moisture deficits than suggested by observational estimates. These biases hamper the model representations of both regional and global water cycles. For example, the Amazon is characterized by a high precipitation recycling ratio, as about one third of the rainfall has previously evaporated from the Amazon itself[34]. In this and other regions strongly reliant on terrestrial ET, exaggerated ET reduction in response to soil moisture deficits in the model could result in excessive drought self-intensification and self-propagation[10,35]. Given that precipitation projections are uncertain due to both internal climate variability and the reliance on parameterizations at subgrid-scales[1], it is crucial to improve the model fidelity of ET to prevent an amplification of this uncertainty through unrealistic land–atmosphere interactions. As the global hydrological cycle is expected to intensify in response to our warming climate[36], although the extent to which this already emerges remains debated[37,38], these biases should disproportionately affect the reliability of future projections.

Owing to the fundamental role of soil moisture in modulating not only water but also energy and carbon fluxes, model biases in water use and limitation propagate beyond the hydrological cycle. Soil moisture–temperature feedbacks are known to amplify hot extremes in most land areas (e.g., Ref[39]), which also emerges clearly in climate projections[40,41]. In fact, it has recently been shown that across much of Europe, air temperature increases are outpaced by even stronger soil temperature trends, suggesting that the heat comes from below[42]. It is challenging to reliably quantify the role of soil moisture–temperature coupling in changing climate, but for certain regions such as the moist tropics, including Amazonia, CMIP6 simulations point to a strong contribution of land feedbacks to extreme heat[43]. Recent work, again based on CMIP6 model experiments, indicates that strong land-atmosphere coupling will become more widespread under increasing atmospheric CO_2, suggesting an amplification of future climate sensitivity to such feedbacks[44]. These findings distinctly rely on the ability of the CMIP6 multi-model ensemble to adequately capture the interactions between land and atmosphere, yet our results indicate systematic deficiencies with respect to how the land surface models make use of the available subsurface water, and how they respond to drought conditions. As such, targeted efforts to improve the representation of these processes in climate models would likely enable more accurate projections of hot and dry extremes.

We remark here that in certain regions, for example the Great Plains and South Asia, the CMIP6 model subset used here underestimates the frequency of soil moisture limitation (Fig. 3). Consequently, in those regions, increases in both the occurrence and magnitude of future heatwaves could be underestimated by current state-of-the-art ESMs. Individual hot and dry events can undo several years' worth of net carbon uptake at regional scales[45], and global soil moisture variability has been shown to dictate the strength of the terrestrial carbon sink[8,9,46], which in turn largely governs the fraction of anthropogenic CO_2 emissions remaining in the atmosphere. Due to this inherent link between land carbon sequestration and climate extremes, model improvements of both subsurface water utilization and limitation could also decrease the intermodel uncertainty of projected carbon uptake and hence long-term climate projections.

In this study, we have highlighted deficiencies in how ESMs represent water storage and soil moisture limitation in climate models. The consistent biases found across CMIP6 models with respect to observations, i.e. underestimated land water storage and overestimated soil moisture limitation, indicate a significant potential for model development. Our analysis illustrates the challenges ESMs face in accurately capturing the specificities of the land water cycle, with significant implications for the simulated land water, energy and carbon fluxes. We note that although the overestimated water limitation could be interpreted as a direct consequence of the underestimated water storage, it is also conceivable that the land component of the ESMs responds too strongly to water stress, reducing evaporation and thereby limiting further soil moisture depletion. This is consistent with other studies pointing to a general overreliance on shallow rather than deep soil moisture in models[24,47] and the stronger drying trends in projections of surface compared to deep soil moisture[48]. Future research into land-climate dynamics under climate change can be supported by focusing on land surface model simulations at flux sites and, in general, using higher frequency data outputs[49]. This would offer a more direct comparison between model predictions and empirical observations, avoiding scale mismatches and thus advancing our understanding of terrestrial water and carbon cycles.

Methods

Data sets

This study investigates water constraints across several models from the Coupled Model Intercomparison Project phase 6[2]. Our focus is on the *Land-Hist* experiment within the Land Model Intercomparison Project (LMIP), which consists in land-only offline simulations over a historical interval improving snow and soil moisture estimates. Sharing the same configuration of *historical* simulations of the parent model within CMIP6, the *Land-Hist* experiment is conceived for diagnosing systematic biases within the land component of ESMs[16].

To benchmark CMIP6 models, we use several observational datasets. For the estimation of the maximum soil moisture depletion in Fig. 1, we use total water storage (TWS) data from the Gravity Recovery and Climate Experiment (GRACE)[17]. TWS accounts for soil moisture, groundwater, surface water, snow and ice and it has been successfully used in previous hydrological studies[50,51]. It is used here as a proxy of total moisture storage. The key advantage of the GRACE dataset lies in its foundation on mass balance principles, ensuring its water balance aligns with that of CMIP6 models. Both CMIP6 models and GRACE operate on this principle, providing consistency in their approach to water balance, despite the CMIP6 models likely not capturing all physical processes perfectly. We use SIF from version 2.6 of the Global Ozone Monitoring Experiment-2 (GOME-2)[52] as a proxy of photosynthetic activity (Fig. 3), consistent with previous studies[30,52,53]. Monthly means are calculated retaining days when the effective cloud fraction is $<30\%$, as described in Ref[30]. SIF is a complementary process of photosynthesis, and it is thus directly related to the photosynthetic rate[54]. We used eddy-covariance data from the FLUXNET2015 dataset[55] complemented with soil moisture simulated with a bucket-type soil water balance model[56] when observational soil moisture from FLUXNET2015 was unavailable or inconsistent, as documented in Ref[26].

We use CMIP6 data from the ETH Zürich CMIP6 next generation (CMIP6ng) archive[57], which adds extra validation for processed variables and consistency among files from different sources. Even though some observational data sets were available at a greater resolution, all data were bilinearly interpolated to a common 2.5° × 2.5° global grid for comparison. We retained pixels with vegetated land using a global land cover dataset from MODIS[58]. To group the vegetated land pixels of the world in meaningful climatic regions (Fig. 2), we use the fourth version of the IPCC WGI reference regions[59]. All analyses were performed using R Statistical Software[60]. To access all code and R packages used in this study, please refer to our published repository on GitHub and Zenodo (see 'Data Availability' section).

Estimating maximum soil moisture depletion

To estimate the maximum soil moisture depletion in CMIP6 models, we used the total column soil moisture (variable 'mrso') at the monthly resolution. We first calculated the difference in annual maximum and minimum soil moisture values, and then selected the greatest difference across all years (Fig. 1). Directly calculating the difference as the maximum minus the minimum soil moisture across all years yielded similar results (Supplementary fig. 7). The initial calculation was chosen because land cover is subject to change over time, making the subtraction of soil moisture values from widely spaced time points potentially not physically meaningful. For the observational map in Fig. 1, we repeated the calculation of the maximum soil moisture depletion with TWS from GRACE (Fig. 1), also used at monthly resolution. The calculation was performed for the years 2003-2014, when both GRACE and CMIP6 data sets were available. GRACE was converted from cm to mm, whereas total column soil moisture was already available in Kg m^{-2} (equivalent to mm H_2O).

To ensure robustness of our analysis, we also estimated the maximum water storage with the cumulative water deficit calculated as in Refs[19,26], using ALEXI and WATCH-WFDEI data as observational benchmark, which confirmed our results (Fig. 1).

To visualize regional biases in CMIP6 predictions, we grouped the results of Fig. 1 by IPCC climate reference regions[59]. We determined the mean of the land water storage across all points within each region, using CMIP6 data. We then compared to the corresponding observational data for the same region (Fig. 2).

Determining moisture limitation thresholds globally with monthly data

We studied the evaporative fraction (EF) as a function of the total column soil moisture (SM, variable 'mrso') using monthly data from CMIP6 models. EF was calculated as the ratio of latent heat flux to net radiation:

$$EF = \frac{latent\ heat\ flux}{R_n} = \frac{\mathrm{hfls}}{(\mathrm{rsds} - \mathrm{rsus}) + (\mathrm{rlds} - \mathrm{rlus})} \quad (2)$$

where 'hfls' (W m^{-2}) is latent heat flux from CMIP6 and 'rsds', 'rsus', 'rlds' and 'rlus' were respectively incoming and outgoing shortwave radiation and incoming and outgoing longwave radiation (W m^{-2}), also from CMIP6. We retained pixels with $R_n > 75$ W m^{-2} to focus on the growing season. We then fitted a segmented linear regression with one breakpoint (also known as "linear-plus-plateau model"[61,62]) to the EF vs SM relationship at each pixel, using R package "segmented"[63]. The pixel-specific estimate of the breaking point θ_{crit} was determined by least-square fit; its value represents the SM threshold up to which EF increases linearly as a function of SM (water-limited regime)[7,61,62]. The percentage of time under water limitation was calculated as the ratio of the number of months with SM < θ_{crit} divided by the total number of months (Fig. 3).

We explored the idea of using the intercept and slope from the segmented regression to quantify water limitation. We decided to maintain our present qualitative methodology (i.e., the fraction of time subjected to water limitation), given the high sensitivity of both the intercept and slope to the underlying assumptions of the segmented regression and the quantity of data points included in the analysis.

The global observational map shown in Fig. 3 was created with GOME-2 SIF[52] data and TWS data from GRACE[17] as a proxy of total column soil moisture. To derive a metric comparable to EF, SIF data were normalized to their maximum value over the entire measurement period, as in Ref.[9]. We focused on monthly data from the growing season by retaining pixels greater than or equal to half of the pixel-specific maximum. Both model and observational analyses were limited to the period from January 2007 to December 2014 (eight years), based on the availability of the observational and modelled datasets.

Determining moisture limitation thresholds at flux tower locations with daily data

We repeated the EF vs SM analysis outlined in the preceding section at the site-scale, using FLUXNET2015 daily data at selected sites (Fig. 4 and Supplementary Fig. 8). We calculated EF using FLUXNET2015 data as $EF = \frac{latent\ heat\ flux}{R_n}$. Due to inconsistencies of measured soil moisture at several FLUXNET2015 sites[26], we simulated soil moisture at eddy-covariance locations with SPLASH, a bucket-type soil water balance mode based on a Priestley-Taylor formulation for ET estimation; with set the water-holding capacity to 220mm[56,64]. We focused on the growing season by retaining site-days with GPP equal or greater than half of the site-specific maximum. We extracted EF and SM data at FLUXNET2015 locations using daily datasets from 2000 to 2014. We used daily CMIP6 data (available only for models UKESM1-0-LL, IPSL-CM6A-LR, EC-Earth3-Veg, and CNRM-ESM2-1) and focused on the grid cell corresponding to the relative FLUXNET2015 site for comparison. We determined the critical threshold θ_{crit} and calculated the percentage of days when SM was less than θ_{crit} relative to the total number of days. When the decrease in the EF was less than 0.3, as indicated by the y-axis intercept compared to its maximum value, we assigned a status of no water limitation (NA).

Data availability

All intermediate data and computer code that support this study are available from the Zenodo Digital Repository: https://zenodo.org/doi/10.5281/zenodo.10810324 (Giardina et al. 2024).

All data used in this study are openly available:

- LMIP-CMIP6 data (see Table S1 and Methods for details of the experiments and run IDs): https://esgf-node.llnl.gov/search/cmip6/ or directly from the ETH Zurich CMIP6 next generation archive: https://zenodo.org/records/3734128
- GRACE land data: https://grace.jpl.nasa.gov/data/get-data/jpl_global_mascons/
- GOME-2 SIF: https://avdc.gsfc.nasa.gov/pub/data/satellite/MetOp/GOME_F
- Ecosystem fluxes and meteorological data: https://fluxnet.org/data/fluxnet2015-dataset/
- Global estimates of maximum CWD determined from ALEXI and WATCH-WFDEI data, augmented using an extreme value distribution: https://zenodo.org/records/5515246

Acknowledgements

The authors extend their gratitude to all data providers who have made this study possible. In particular, we want to acknowledge the FLUXNET community, for their role in making the FLUXNET2015 dataset available.

Author Contributions

F.G. wrote the main manuscript in collaboration with R.S.P. and D.L.S. F.G. prepared figures. F.G., S.I.S. and R.S.P. designed the study. F.G. performed the analysis in collaboration with R.S.P. All authors reviewed and edited the manuscript.

Competing Financial Interests

The authors declare no competing financial interests.

References

1. Seneviratne, S. I. *et al.* Weather and Climate Extreme Events in a Changing Climate. *Climate Change 2021: The Physical Science Basis. Contribution of Working Group I to the Sixth Assessment Report of the Intergovernmental Panel on Climate Change* **Cambridge**, (2021).
2. Eyring, V. *et al.* Overview of the Coupled Model Intercomparison Project Phase 6 (CMIP6) experimental design and organization. *Geosci Model Dev* **9**, 1937–1958 (2016).
3. Meinshausen, M. *et al.* The shared socio-economic pathway (SSP) greenhouse gas concentrations and their extensions to 2500. *Geosci Model Dev* **13**, 3571–3605 (2020).
4. Tebaldi, C. & Knutti, R. The use of the multi-model ensemble in probabilistic climate projections. *Philosophical Transactions of the Royal Society A: Mathematical, Physical and Engineering Sciences* vol. 365 2053–2075 Preprint at https://doi.org/10.1098/rsta.2007.2076 (2007).
5. Tokarska, K. B. *et al.* Past warming trend constrains future warming in CMIP6 models. *Sci Adv* **6**, 9549–9567 (2020).
6. Qiao, L., Zuo, Z. & Xiao, D. Evaluation of Soil Moisture in CMIP6 Simulations. *J Clim* **35**, 779–800 (2022).
7. Seneviratne, S. I. *et al.* Investigating soil moisture-climate interactions in a changing climate: A review. *Earth Sci Rev* **99**, 125–161 (2010).
8. Humphrey, V. *et al.* Sensitivity of atmospheric CO2 growth rate to observed changes in terrestrial water storage. *Nature* **560**, 628–631 (2018).
9. Green, J. K. *et al.* Large influence of soil moisture on long-term terrestrial carbon uptake. *Nature* **565**, 476–479 (2019).
10. Miralles, D. G., Gentine, P., Seneviratne, S. I. & Teuling, A. J. Land–atmospheric feedbacks during droughts and heatwaves: state of the science and current challenges. *Ann N Y Acad Sci* **1436**, 19–35 (2019).
11. Budyko, M. I. *Climate and Life*. (Academic Press, 1974).
12. Humphrey, V., Gudmundsson, L. & Seneviratne, S. I. Assessing Global Water Storage Variability from GRACE: Trends, Seasonal Cycle, Subseasonal Anomalies and Extremes. *Surveys in Geophysics* vol. 37 357–395 Preprint at https://doi.org/10.1007/s10712-016-9367-1 (2016).

13. Schwingshackl, C., Hirschi, M. & Seneviratne, S. I. Quantifying spatiotemporal variations of soil moisture control on surface energy balance and near-surface air temperature. *J Clim* **30**, 7105–7124 (2017).

14. García-García, A., Cuesta-Valero, F. J., Beltrami, H. & Smerdon, J. E. Characterization of Air and Ground Temperature Relationships within the CMIP5 Historical and Future Climate Simulations. *Journal of Geophysical Research: Atmospheres* **124**, 3903–3929 (2019).

15. Sippel, S. *et al.* Refining multi-model projections of temperature extremes by evaluation against land-Atmosphere coupling diagnostics. *Earth System Dynamics* **8**, 387–403 (2017).

16. Van Den Hurk, B. *et al.* LS3MIP (v1.0) contribution to CMIP6: The Land Surface, Snow and Soil moisture Model Intercomparison Project - Aims, setup and expected outcome. *Geosci Model Dev* **9**, 2809–2832 (2016).

17. Landerer, F. W. & Swenson, S. C. Accuracy of scaled GRACE terrestrial water storage estimates. *Water Resour Res* **48**, (2012).

18. Liu, L. *et al.* Increasingly negative tropical water–interannual CO2 growth rate coupling. *Nature* **618**, 755–760 (2023).

19. Stocker, B. D. *et al.* Global patterns of water storage in the rooting zones of vegetation. *Nat Geosci* **16**, 250–256 (2023).

20. Hain, C. R. & Anderson, M. C. Estimating morning change in land surface temperature from MODIS day/night observations: Applications for surface energy balance modeling. *Geophys Res Lett* **44**, 9723–9733 (2017).

21. Anderson, M. C., Norman, J. M., Diak, G. R., Kustas, W. P. & Mecikalski, J. R. A two-source time-integrated model for estimating surface fluxes using thermal infrared remote sensing. *Remote Sens Environ* **60**, 195–216 (1997).

22. Weedon, G. P. *et al.* The WFDEI meteorological forcing data set: WATCH Forcing Data methodology applied to ERA-Interim reanalysis data. *Water Resour Res* **50**, 7505–7514 (2014).

23. Ukkola, A. M. *et al.* Land surface models systematically overestimate the intensity, duration and magnitude of seasonal-scale evaporative droughts. *Environmental Research Letters* **11**, 104012 (2016).

24. Zhao, M., A, G., Liu, Y. & Konings, A. G. Evapotranspiration frequently increases during droughts. *Nat Clim Chang* **12**, 1024–1030 (2022).

25. Teuling, A. J., Seneviratne, S. I., Williams, C. & Troch, P. A. Observed timescales of evapotranspiration response to soil moisture. *Geophys Res Lett* **33**, 0–4 (2006).
26. Giardina, F., Gentine, P., Konings, A. G., Seneviratne, S. I. & Stocker, B. D. Diagnosing evapotranspiration responses to water deficit across biomes using deep learning. *New Phytologist* **240**, 968–983 (2023).
27. Green, J. K., Berry, J., Ciais, P., Zhang, Y. & Gentine, P. Amazon rainforest photosynthesis increases in response to atmospheric dryness. *Sci Adv* **6**, (2020).
28. Pagán, B., Maes, W., Gentine, P., Martens, B. & Miralles, D. Exploring the Potential of Satellite Solar-Induced Fluorescence to Constrain Global Transpiration Estimates. *Remote Sens (Basel)* **11**, 413 (2019).
29. Pan, Y. *et al.* A large and persistent carbon sink in the world's forests. *Science (1979)* **333**, 988–993 (2011).
30. Giardina, F. *et al.* Tall Amazonian forests are less sensitive to precipitation variability. *Nat Geosci* **11**, 405–409 (2018).
31. Huntingford, C. *et al.* Simulated resilience of tropical rainforests to CO2-induced climate change. *Nat Geosci* **6**, 268–273 (2013).
32. Kennedy, D. *et al.* Implementing Plant Hydraulics in the Community Land Model, Version 5. *J Adv Model Earth Syst* **11**, 485–513 (2019).
33. Lawrence, D. M. *et al.* The Community Land Model Version 5: Description of New Features, Benchmarking, and Impact of Forcing Uncertainty. *J Adv Model Earth Syst* **11**, 4245–4287 (2019).
34. Dominguez, F. *et al.* Amazonian Moisture Recycling Revisited Using WRF With Water Vapor Tracers. *Journal of Geophysical Research: Atmospheres* **127**, e2021JD035259 (2022).
35. Schumacher, D. L., Keune, J., Dirmeyer, P. & Miralles, D. G. Drought self-propagation in drylands due to land–atmosphere feedbacks. *Nat Geosci* **15**, 262–268 (2022).
36. Allen, M. R. & Ingram, W. J. Constraints on future changes in climate and the hydrologic cycle. *Nature* vol. 419 224–232 Preprint at https://doi.org/10.1038/nature01092 (2002).
37. Koutsoyiannis, D. Revisiting the global hydrological cycle: Is it intensifying? *Hydrol Earth Syst Sci* **24**, 3899–3932 (2020).
38. Akhoudas, C. H. *et al.* Isotopic evidence for an intensified hydrological cycle in the Indian sector of the Southern Ocean. *Nat Commun* **14**, 1234567890 (2023).

39. Mueller, B. & Seneviratne, S. I. Hot days induced by precipitation deficits at the global scale. *Proc Natl Acad Sci U S A* **109**, 12398–12403 (2012).
40. Vogel, M. M. *et al.* Regional amplification of projected changes in extreme temperatures strongly controlled by soil moisture-temperature feedbacks. *Geophys Res Lett* **44**, 1511–1519 (2017).
41. Vogel, M. M., Zscheischler, J. & Seneviratne, S. I. Varying soil moisture-atmosphere feedbacks explain divergent temperature extremes and precipitation projections in central Europe. *Earth System Dynamics* **9**, 1107–1125 (2018).
42. García-García, A. *et al.* Soil heat extremes can outpace air temperature extremes. *Nat Clim Chang* **13**, 1237–1241 (2023).
43. Dirmeyer, P. A., Sridhar Mantripragada, R. S., Gay, B. A. & Klein, D. K. D. Evolution of land surface feedbacks on extreme heat: Adapting existing coupling metrics to a changing climate. *Front Environ Sci* **10**, 949250 (2022).
44. Hsu, H. & Dirmeyer, P. A. Soil moisture-evaporation coupling shifts into new gears under increasing CO2. *Nat Commun* **14**, 1–9 (2023).
45. Ciais, P. *et al.* Europe-wide reduction in primary productivity caused by the heat and drought in 2003. *Nature* **437**, 529–533 (2005).
46. Padrón, R. S., Gudmundsson, L., Liu, L., Humphrey, V. & Seneviratne, S. I. Drivers of intermodel uncertainty in land carbon sink projections. *Biogeosciences* **19**, 5435–5448 (2022).
47. Dong, J., Lei, F. & Crow, W. T. Land transpiration-evaporation partitioning errors responsible for modeled summertime warm bias in the central United States. *Nat Commun* **13**, 1–8 (2022).
48. Berg, A., Sheffield, J. & Milly, P. C. D. Divergent surface and total soil moisture projections under global warming. *Geophys Res Lett* **44**, 236–244 (2017).
49. Findell, K. L. *et al.* Accurate assessment of land–atmosphere coupling in climate models requires high-frequency data output. *Geosci Model Dev* **17**, 1869–1883 (2024).
50. Jiang, W. *et al.* Annual variations of monsoon and drought detected by GPS: A case study in Yunnan, China. *Sci Rep* **7**, 1–10 (2017).
51. Yang, Y. *et al.* GRACE satellite observed hydrological controls on interannual and seasonal variability in surface greenness over mainland Australia. *J Geophys Res Biogeosci* **119**, 2245–2260 (2014).

52. Joiner, J. *et al.* Global monitoring of terrestrial chlorophyll fluorescence from moderate-spectral-resolution near-infrared satellite measurements: methodology, simulations, and application to GOME-2. *Atmos Meas Tech* **6**, 2803–2823 (2013).
53. Frankenberg, C. *et al.* New global observations of the terrestrial carbon cycle from GOSAT: Patterns of plant fluorescence with gross primary productivity. *Geophys Res Lett* **38**, 1–6 (2011).
54. Porcar-Castell, A. *et al.* Linking chlorophyll a fluorescence to photosynthesis for remote sensing applications: Mechanisms and challenges. *J Exp Bot* **65**, 4065–4095 (2014).
55. Pastorello, G. *et al.* The FLUXNET2015 dataset and the ONEFlux processing pipeline for eddy covariance data. *Sci Data* **7**, 225 (2020).
56. Davis, T. W. *et al.* Simple process-led algorithms for simulating habitats (SPLASH v.1.0): Robust indices of radiation, evapotranspiration and plant-available moisture. *Geosci Model Dev* **10**, 689–708 (2017).
57. Brunner, L., Hauser, M. & Beyerle, R. L. and U. The ETH Zurich CMIP6 next generation archive: technical documentation. Preprint at https://doi.org/10.5281/zenodo.3734128 (2020).
58. Friedl, M. A. *et al.* MODIS Collection 5 global land cover: Algorithm refinements and characterization of new datasets. *Remote Sens Environ* **114**, 168–182 (2010).
59. Iturbide, M. *et al.* An update of IPCC climate reference regions for subcontinental analysis of climate model data: definition and aggregated datasets. *Earth Syst Sci Data* **12**, 2959–2970 (2020).
60. R Core Team. R: A language and environment for statistical computing. R Foundation for Statistical Computing, Vienna, Austria. URL https://www.R-project.org/. (2023).
61. Fu, Z. *et al.* Critical soil moisture thresholds of plant water stress in terrestrial ecosystems. *Sci Adv* **8**, 7827 (2022).
62. Fu, Z. *et al.* Uncovering the critical soil moisture thresholds of plant water stress for European ecosystems. *Glob Chang Biol* **28**, 2111–2123 (2022).
63. Muggeo, V. M. R. Estimating regression models with unknown break-points. *Stat Med* **22**, 3055–3071 (2003).
64. Orth, R., Koster, R. D. & Seneviratne, S. I. Inferring soil moisture memory from streamflow observations using a simple water balance model. *J Hydrometeorol* **14**, 1773–1790 (2013).